Earthline Journal of Mathematical Sciences
E-ISSN: 2581-8147
Volume 10, Number 2, 2022, Pages 241-270
https://doi.org/10.34198/ejms.10222.241270

Magnetized Flow of Electrically Induced Maxwell Nanofluid over Reactive Stretching Plate with Thermal Stratification

Christian John Etwire[1,*], Ibrahim Yakubu Seini[2] and Oluwole Daniel Makinde[3]

[1] School of Mathematical Sciences, C.K. Tedam University of Technology and Applied Sciences, P.O. Box 24, Navrongo, UER, Ghana
e-mail: jecpapa@yahoo.com

[2] School of Engineering, University for Development Studies, Nyankpala Campus, P.O. Box 1882, Tamale, Ghana
e-mail: yakubuseini@yahoo.com

[3] Faculty of Military Science, Stellenbosch University, Private Bag X2, Saldanha 7395, South Africa
e-mail: makinded@gmail.com

Abstract

Effects of thermal stratification on magnetized flow of electrically induced Maxwell nanofluid over reactive stretching plate have been analyzed. The nonlinear ordinary differential equations governing the flow problem were obtained by applying Similarity transformation. The resulting model was then solved with the aid of the fourth order Runge-Kutta algorithm along with the shooting technique. Results for pertinent flow parameters were tabulated and analyzed graphically. The Richardson number was noted to appreciate the momentum boundary layer thickness but it decayed both the thermal and solutal boundary layer thicknesses.

Introduction

The study of the transport mechanism of electro-magnetohydrodynamic flow of Maxwell nanofluid past stretching surface is gaining interest from the scientific world due to the promising benefits it presents to the electronic, automobile, petrochemical, biomedical and tribological industries. It is significant for magnetic reconnection, magnetic drug targeting, plasma switches and confinement, z-pinch, liquid-metal cooling of nuclear reactors, ion thrusters and electromagnetic casting. As a result of these

Received: June 7, 2022; Accepted: June 29, 2022

2020 Mathematics Subject Classification: 76W05.

Keywords and phrases: magnetized flow, Maxwell, stratification, reactive, nanofluid.

*Corresponding author

applications, researchers and scientists have examined the flow dynamics of Maxwell nanofluid. Ramzan et al. [1] provided an optimal solution to mixed convective flow of Maxwell nanofluid over a porous vertical stretching surface and noted the Deborah number to enhance Sherwood number but it decayed both the Nusselt number and velocity profile. Ibrahim [2] analysed magnetohydrodynamic stagnation point flow of upper-convected Maxwell fluid past a stretching sheet containing nanoparticles with heat transfer and convective heating and found the Deborah number to appreciate the momentum boundary layer thickness and decayed the thermal boundary layer thickness. Elbashbeshy et al. [3] discussed the heat and mass transport potential of a Maxwell nanofluid over a stretching surface embedded in porous media and noted the Deborah number to enhance the skin friction coefficient and concentration profiles but depleted the velocity of the nanofluid. Mushtaq [4] found the fluid relaxation time parameter to weaken the momentum boundary layer thickness in Buoyancy induced stagnation-point flow of Maxwell fluid. Sravanthi and Gorla [5] examined MHD Maxwell nanofluid flow past a convectively heated exponentially stretching sheet with the effects of heat source/sink and chemical reaction. While Sushma et al. [6] discussed the effect of non-uniform heat Source/Sink and external magnetic field on Maxwell nanofluid flow past a stretching sheet. Ahmed et al. [7] noted the velocity profile to deplete with both the Deborah number and magnetic field parameter in Magnetohydrodynamic flow of Maxwell nanofluid over a porous stretching surface with non-Linear thermal radiation and heat transfer mechanism. Farooq et al. [8] studied the effect of nanomaterials on MHD flow of Maxwell fluid over an exponentially stretching surface. Aziz and Shams [9] observed the magnetic field, Maxwell and permeability parameters to enhance the velocity of the flow in slip MHD flow of Maxwell nanofluid with entropy generation and varying heat generation mechanisms. Ibrahim and Negera [10] examined the impact of slip on chemically reacting MHD flow of upper-convected Maxwell nanofluid over a stretching sheet.

Thermal stratification poses a threat to the thermal management of industrial processes and devices as it can increase the heat built-up and consequently limit their performance. For instance, the cooling mechanism of air conditioners, refrigerators, nuclear power plants, radiators, engines and transformers involve thermal stratification. Inadequate cooling of these engineering designs constrain their functionality. To enhance the performance of these devices, many researchers have studied the impact of thermal stratification on flow dynamics of coolants. Singh and Kumar [11] investigated the role of dual stratification in MHD free convection flow of Micropolar fluid with chemical

reaction and heat generation and noted both the thermal and solutal stratification parameters to deplete the velocity, temperature and concentration of the nanofluid. Abbasi et al. [12] discussed the impact of dual stratification on mixed convection flow of Maxwell nanofluid with heat generation/absorption. While Ganesh et al. [13] studied the combined effect of viscous and Ohmic dissipation on thermally stratified hydromagnetic Darcy-Forchheimer flow of nanofluid past a stretching/shrinking sheet in a porous medium with second order slip. Ramzan et al. [14] also found both the thermal and solutal stratification parameter to deplete the temperature and concentration of the flow in a radiating and double stratification stagnation point flow of Powell-Eyring magneto-nanofluid past a stretching cylinder. Daniel et al. [15] explored MHD flow of radiating nanofluid past nonlinear stretching sheet with thermal stratification and variable thickness. Sreelakshmi et al. [16] investigated dual stratification in Darcy-Forchheimer flow of a Maxwell nanofluid past a Stretching Surface. The role of double stratification on magnetohydrodynamic flow of squeezed Maxwell nanofluid with convective conditions was examined by Farooq et al. [17]. Ramzan et al. [18] observed the thermal stratification parameter to decay the thermal boundary layer thickness in homogeneous-heterogeneous reactions of thermally stratified Darcy Forchheimer flow over a moving thin needle with non-uniform heat source/sink. Khashi et al. [19] examined the effect of thermal stratification on stagnation point flow of hybrid nanofluid past a permeable vertical stretching/shrinking cylinder.

It is evident from the surveyed literature that study on flow dynamics of Maxwell nanofluid over reactive surface is limited. Hence, this paper intends to explore the effects of electric and magnetic fields on Maxwell nanofluid flow over reactive stretching plate with thermal stratification. Since reactive surfaces can alter the cooling efficacy of coolants. The subsequent sections of the paper will cover the mathematical model, similarity transformation, computational method, results and discussions and conclusions.

Mathematical Model

Consider a steady and incompressible flow of electrically conducting Maxwell nanofluid over a porous reactive stretching plate with thermal stratification. The flow is confined in xy plane as shown in Figure 1 and exposed to the combined impact of external electric and magnetic fields of strengths E_0 and B_0 respectively. The effects of the induced electric and magnetic field current is negligible due to the assumption that the Reynolds number is very small. The velocity of the stretching surface is taken to be $u = bx$. The stretching plate is considered to have a temperature of $T_w = T_0 + B_1 x$ and

concentration of C_w. The ambient nanofluid has a stratified temperature of $T_\infty = T_0 + B_2 x$ and concentration of C_∞. The coefficient of the mass transport of the flow is given by h_m.

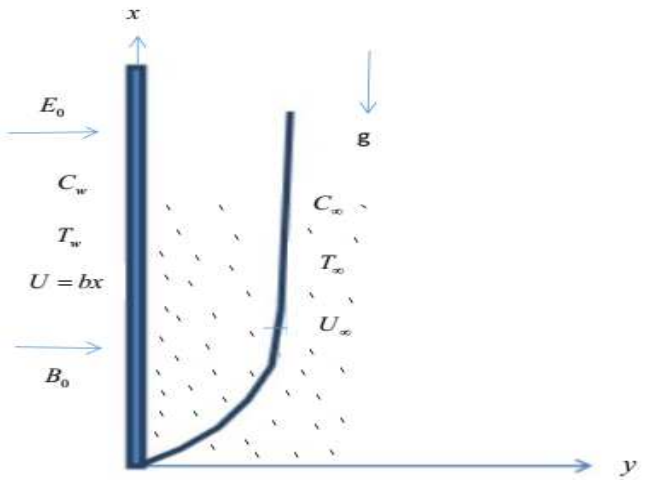

Figure 1: Flow diagram.

By the assumptions and employing the boundary layer approximations, the continuity, momentum, energy and concentration equations modeling the flow problem can be expressed as;

$$\frac{\partial u}{\partial x} + \frac{\partial v}{\partial y} = 0, \tag{1}$$

$$u\frac{\partial u}{\partial x} + v\frac{\partial u}{\partial y} + \lambda_1\left(u^2\frac{\partial^2 u}{\partial x^2} + v^2\frac{\partial^2 u}{\partial y^2} + 2uv\frac{\partial^2 u}{\partial x \partial y}\right)$$
$$= \upsilon\frac{\partial^2 u}{\partial y^2} - \frac{\sigma B_0}{\rho_f}\left(B_0 u - E_0 + \lambda_1 B_0 v\frac{\partial u}{\partial y}\right) - \frac{\upsilon}{k}u$$
$$+\frac{1}{\rho_f}\left[\rho_{f\infty}\beta g(1 - C_\infty)(T - T_\infty) - g(\rho_p - \rho_{f\infty})(C - C_\infty)\right], \tag{2}$$

$$u\frac{\partial T}{\partial x} + v\frac{\partial T}{\partial y} = \alpha\frac{\partial^2 T}{\partial y^2} + \tau\left(D_B\frac{\partial C}{\partial y}\frac{\partial T}{\partial y} + \frac{D_T}{T_\infty}\left(\frac{\partial T}{\partial y}\right)^2\right) + \frac{\sigma}{(\rho C)_f}(B_0 u - E_0)^2, \tag{3}$$

$$u\frac{\partial C}{\partial x} + v\frac{\partial C}{\partial y} = D_B\frac{\partial^2 C}{\partial y^2} + \frac{D_T}{T_\infty}\frac{\partial^2 T}{\partial y^2}, \tag{4}$$

subject to the boundary conditions

$$u(x,0) = bx,\ \ v(x,0) = -v_w,\ \ T(x,0) = T_w = T_0 + A_1 x,\ \ -D_B\frac{\partial C}{\partial y} = h_m(C_w - C),$$
$$\text{at } y = 0$$

$$u(x,\infty)\to 0,\ \ \frac{\partial u}{\partial y}\to 0,\ \ T(x,\infty)\to T_\infty = T_0 + A_2 x,\ \ C(x,\infty)\to C_\infty,\ \ \text{as}\ \ y\to\infty \quad (5)$$

where u and v are respectively the x and y components of the flow velocity, υ is the kinematic viscosity of the nanofluid, ρ_f is the density of the nanofluid, λ_1 is the relaxation time parameter of the nanofluid, α is the thermal diffusivity, σ is the electrical conductivity, β is the volume expansion coefficient, k' is the permeability of the porous media, T is the temperature of the nanofluid, ρ_p is the density of the nanoparticles, g is the acceleration due to gravity, $(\rho C)_f$ is the heat capacity of the nanofluid, $\tau = \frac{(\rho C)_f}{(\rho C)_p}$, $(\rho C)_p$ is the heat capacity of the nanoparticles, D_B is the Brownian diffusion coefficient, C is the concentration and D_T is the thermophoresis diffusion coefficient.

Similarity Transformations

Defining the stream function, $\psi(x,y)$ in the obvious way as;

$$u = \frac{\partial \psi}{\partial y}\ \ \text{and}\ \ v = -\frac{\partial \psi}{\partial x}. \quad (6)$$

Equation (1) is satisfied automatically by equation (6). A solution of equations (2)-(4) is achieved by employing an independent dimensionless variable, η, a stream function, ψ, in terms of a dependent variable $f(\eta)$, a dimensionless temperature $\theta(\eta)$ and a dimensionless concentration $\phi(\eta)$ as;

$$\eta = y\sqrt{\frac{b}{\upsilon_f}},\ \ \psi = \sqrt{b\upsilon_f}\,x f(\eta),\ \ \theta(\eta) = \frac{T-T_\infty}{T_w - T_0},\ \ \phi(\eta) = \frac{C-C_\infty}{C_w - C_\infty}. \quad (7)$$

Putting the relevant terms into equations (2)-(4) give the nonlinear differential equations as;

$$f''' + ff'' - f'^2 - \gamma\left(f^2 f''' - 2ff'f''\right) - M\left(f' - \gamma f'' - E\right) + Ri(\theta - N_r\phi) - K^* f' = 0, \quad (8)$$

$$\theta'' + Pr\left(f\theta' + N_b\theta'\varphi' + N_t\theta'^2 - f'\theta - S_T f'\right) + Ec\,Pr\,M\,(f' - E)^2 = 0, \quad (9)$$

$$\phi'' - Le\,Pr\,f\,\phi' + \frac{N_t}{N_b}\theta'' = 0, \quad (10)$$

subject to the boundary conditions

$$f'(0) = 1,\ f(0) = S,\ \theta(0) = 1 - S_T,\ \phi'(0) = -Da\left(1 - \phi(0)\right)\ \text{at}\ \eta = 0,$$
$$f'(\infty)\to 0,\ f''(\infty)\to 0,\ \theta(\infty)\to 0,\ \phi(\infty)\to 0,\ \text{as}\ \eta\to\infty, \quad (11)$$

where the prime symbol depicts differentiation with respect to η, $K^* = \frac{\upsilon_f}{bk'}$ is the permeability parameter, $Pr = \frac{\upsilon_f}{\alpha_f}$ is the Prandtl number, $M = \frac{\sigma B_o^2}{\rho_f b}$ is the magnetic field parameter, $S = -\frac{v_w}{\sqrt{b\upsilon_f}}$ is the suction parameter and $\gamma = b\lambda_1$ is the Deborah number, $Ri = \frac{Gr}{Re^2}$ is the Richardson number, $E = \frac{E_o}{u_w B_o}$ is the electric field parameter, $Gr = \frac{\rho_{f\infty} g\beta(1-C_\infty)(T_w-T_o)x^2}{\rho_f \upsilon^2}$ is the Grashof number, $S_T = \frac{A_2}{A_1}$ is the thermal stratification parameter, $Nr = \frac{(\rho_f-\rho_{f\infty})(C_w-C_\infty)}{\rho_{f\infty}\beta(1-C_\infty)(T_w-T_0)}$ is the buoyancy ratio parameter, $N_b = \frac{(\rho c)_p D_B(C_w-C_\infty)}{(\rho c)_f \upsilon}$ is the Brownian motion parameter, $Le = \frac{\alpha_f}{D_B}$ is the Lewis number, $N_t = \frac{(\rho c)_p D_T(T_w-T_o)}{(\rho c)_f T_\infty \upsilon}$ is the Thermophoresis parameter, $Ec = \frac{u_w^2}{(c_p)_f(T_w-T_o)}$ is the Eckert number and $Da = \frac{h_m}{D_B}\sqrt{\frac{\upsilon}{b}}$ is the Damkohler number. The skin-friction coefficient (C_f), Nusselt number (Nu) and Sherwood number (Sh) which are of relevance to engineers are respectively given by;

$$C_f = \frac{\tau_w}{\rho_f u_w^2}, \quad Nu = \frac{xq_w}{k_f(T_w-T_\infty)} \text{ and } Sh = \frac{xq_m}{D_B(C_w-C_\infty)}, \tag{12}$$

where τ_w, q_w and q_m are the wall shear stress, heat flux and mass flux respectively which are defined as;

$$\tau_w = \mu_f \frac{\partial u}{\partial y}\Big|_{y=0}, \quad q_w = -k_f \frac{\partial T}{\partial y}\Big|_{y=0} \text{ and } q_m = -D_B \frac{\partial C}{\partial y}\Big|_{y=0}. \tag{13}$$

Plugging equation (13) into equation (12) gives;

$$C_f = \frac{1}{\sqrt{Re_x}} f''(0), \tag{14}$$

$$Nu = -\sqrt{Re_x}\theta'(0), \tag{15}$$

$$Sh = -\sqrt{Re_x}\varphi'(\eta) \tag{16}$$

where $Re_x = \frac{U_w x}{\upsilon_f}$ is the local Reynolds number.

Computational Method

By letting;

$$f = x_1, f' = x_2, f'' = x_3, f''' = x_4, \theta = x_5, \theta' = x_6, \theta'' = x_7, \phi = x_8, \phi' = x_9. \tag{17}$$

The flow equations are reduced to first order system of differential equations by substituting equation (17) into equations (8)-(11) to obtain;

$$f' = x_1',$$
$$f'' = x_2',$$
$$f''' = x_3' = \frac{1}{1-\gamma x_1^2}(M(x_2 - \gamma x_3 - E) - \beta_o(x_5 - N_r x_8) + K^* x_2 + x_2^2 - x_1 x_3 - 2\gamma x_1 x_2 x_3),$$
$$\theta' = x_5',$$
$$\theta'' = x_6' = -Pr(x_1 x_6 + N_b x_6 x_9 + N_t x_6^2 - x_2 x_5 - S_T x_2) - Ec\,Pr\,M\,(x_2 - E)^2,$$
$$\phi' = x_8',$$
$$\phi'' = x_9' = Le\,Pr\,x_1\,x_9 - \frac{N_t}{N_b}x_7, \tag{18}$$

subject to the boundary conditions,

$$x_2 = 1, x_1 = S, x_5 = 1 - S_T, x_9 = Da(1-r), x_2 = p, x_3 = j, x_5 = q, x_8 = r. \tag{19}$$

The system is solved by employing the fourth order Runge Kutta algorithm along with the Shooting technique.

Results and Discussions

The flow model was authenticated by comparing its results for the Nusselt number depicted by $(-\theta'(0))$ with Gorla and Sidawi [20] for different Prandtl number (Pr) with $M = K^* = S = \gamma = E = \beta_o = S_T = N_r = N_b = Le = N_t = Ec = Da = 0$. The comparison is illustrated in Table 1.

Table 1: Computations showing comparison with Gorla and Sidawi [20].

	Gorla and Sidawi [20]	**Present Work**
Pr	$-\theta'(0)$	$-\theta'(0)$
0.7	0.4539	0.4539
2.0	0.9113	0.9114
7.0	1.8954	1.8954

Numerical Results

The role of the thermophysical parameters on the skin friction coefficient $(-f''(0))$, Nusselt number $(-\theta'(0))$ and Sherwood number $\theta'(0)$ are given in Table 2.

Table 2: Computation showing $(-f''(0))$, $(-\theta'(0))$ and $\phi'(0)$ for different parameter values.

γ	Ri	S_T	Da	Le	N_b	N_t	N_r	M	E	Pr	S	$K*$	Ec	$-f''(0)$	$-\theta'(0)$	$\phi'(0)$
0.1	1	0.1	1	0.1	0.1	0.1	0.1	0.1	0.1	1	0.1	0.1	0.1	0.879758	0.997508	0.140774
0.2														0.914789	0.985572	0.165315
	2													0.556883	1.057084	-0.151054
	3													0.254843	1.099899	-0.264404
		0.3												0.987422	0.880792	0.120146
		0.5												1.095658	0.759425	0.109136
			3											0.876996	0.998166	0.217127
			5											0.876041	0.998394	0.243563
				0.4										0.923782	0.952229	0.690070
				0.7										0.982343	0.878261	1.510805
					0.3									0.874070	0.962585	0.165794
					0.5									0.975382	0.537947	2.465919
						0.3								0.879758	0.997508	0.140774
						0.5								0.879758	0.997508	0.140774
							0.2							0.900235	1.001802	-0.196614
							0.3							0.919928	1.000728	-0.307751
								0.2						0.965647	0.950109	0.647348
								0.3						1.046460	0.902169	1.159589
									0.3					0.957525	0.927628	1.091848
									0.5					1.036045	0.841945	2.170893
										3				1.035425	1.913889	2.099475
										5				1.118880	2.500018	0.595750
											0.2			0.947990	1.040187	0.134600
											0.3			1.022411	1.083944	0.134597
												0.4		1.008841	0.971408	0.185349
												0.7		1.128757	0.947030	0.231413
													0.3	0.878617	0.987306	1.146814
													0.5	0.877462	0.977089	0.152722

The Deborah number, Lewis number, Brownian motion parameter, magnetic field parameter, electric field parameter and permeability parameter are seen to increase both the skin friction coefficient and Sherwood number but they decreased the Nusselt number. While appreciating values of the Richardson number increased the Nusselt number but it depleted both the Sherwood number and skin friction coefficient. The thermal stratification and buoyancy ratio parameters enhanced the skin friction coefficient but it decreased the intensities of both the Nusselt and Sherwood numbers. A reverse effect is noted with the Damkohler number. However, the thermophoresis parameter was observed not to influence the intensities of the skin friction coefficient, Nusselt number and Sherwood number. The combined effects of the Prandtl number and suction parameter strengthened the intensities of both the Nusselt number and skin friction coefficient but it decayed the Sherwood number. A counteracting effect is observed with the Eckert number.

Graphical Results

The effects of the thermal stratification parameter on the velocity, temperature and concentration profiles are portrayed in Figures 2-4. It is noted that a rise in the thermal stratification parameter depletes the velocity, temperature and concentration of the nanofluid as well as the respective momentum, thermal and solutal boundary layer thicknesses. The thermal stratification parameter causes temperature deficit across the surface of the plate and this limits the transport potential of the nanofluid. Similar behaviour is evident in Figures 5-7 as the suction parameter is enhanced. A hike in the suction parameter impedes the formation of the boundary layer. Figures 8-13 portray the effect of the magnetic and electric field parameters on the velocity, temperature and concentration profiles. The combined effect of these parameters increased both the thermal and solutal boundary layer thickness while they weaken the momentum boundary layer thickness. Physically, a hike in both the magnetic and electric fields produces a Lorentz force that depletes the velocity of the nanofluid. The resistive forces also increase the heat built-up thereby increasing the temperature and concentration of the nanofluid. The permeability parameter is also found in Figures 14-16 to decay the momentum boundary layer thickness but enhanced both the thermal and solutal boundary layer thickness. Figures 17-19 indicate the influence of the Eckert number on the velocity, temperature and concentration profiles. The Eckert number is found to appreciate both the momentum and thermal boundary layer thicknesses but it degrades the solutal boundary layer thickness as a result of the internal frictional forces of the nanofluid. Opposing trend was found in Figures 20-22 with regards to the momentum, thermal and solutal boundary layer thickness as the Prandtl number was adjusted upward. Figures 23-24 scrutinize the impact of the Buoyancy ratio parameter on the velocity and concentration profiles. The buoyancy ratio parameter is found to decay both the momentum and solutal boundary layer thicknesses. This parameter strengthens the Buoyancy forces which retard the velocity of the nanofluid and surface mass transfer rate. The Deborah number is also noted in Figures 25-26 to degrade both the momentum and solutal boundary layer thicknesses. The Deborah number makes the nanofluid viscous and this slows the velocity and mass diffusion rate of the nanofluid. The impact of the Brownian motion parameter on the velocity, temperature and concentration profiles are presented in Figures 27-29. The Brownian motion parameter is seen to thicken the momentum, thermal and solutal boundary layer thicknesses. The Brownian motion parameter basically increases the internal heat generation due to the random collisions of the nanoparticles which appreciates the velocity and temperature of the nanofluids.

Figure 30 depicts the impact of the Lewis number on the concentration profile. The Lewis number is found to enhance the concentration of the nanofluid and solutal boundary layer thickness. Higher values of the Lewis number generally enhance the thermal diffusion potential of the nanofluid but the reactive stretching surface decays this effect thereby decreasing the concentration gradient across the boundary layer. The Damkohler number is noted in Figure 31 to decrease the concentration of the nanofluid and solutal boundary layer thickness. This is because the Damkohler number physically promotes the reaction rate but the forced convection enhances the convective mass transfer rate. Figures 32-34 denote the impact of the Richardson number on the velocity, temperature and concentration profiles. The velocity of the nanofluid is increased while the temperature and concentration of the nanofluid are decreased with the Richardson number. An increase in the Richardson number physically enhances the buoyancy which thickens the momentum boundary layer thickness but it depletes both the thermal and solutal boundary layer thicknesses.

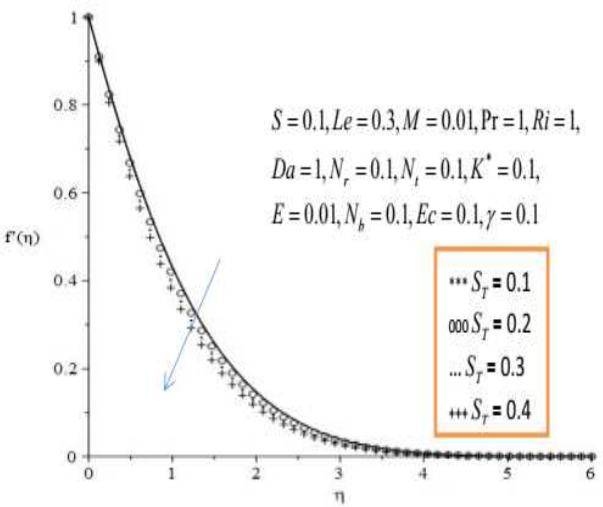

Figure 2: The effect of the thermal stratification parameter on the velocity profile.

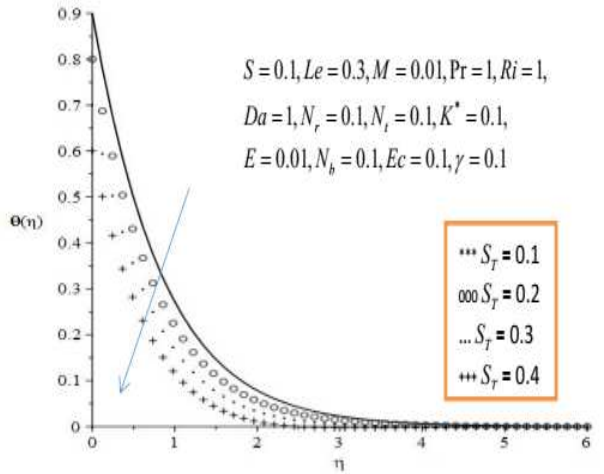

Figure 3: The effect of the thermal stratification parameter on the temperature.

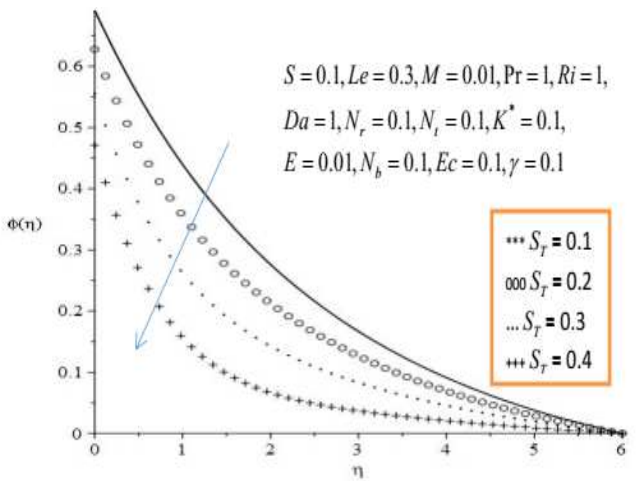

Figure 4: The effect of the thermal stratification parameter on the concentration profile.

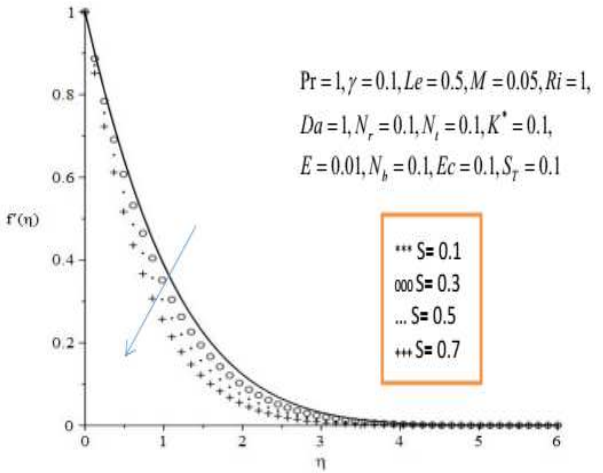

Figure 5: The effect of the suction parameter on the velocity profile.

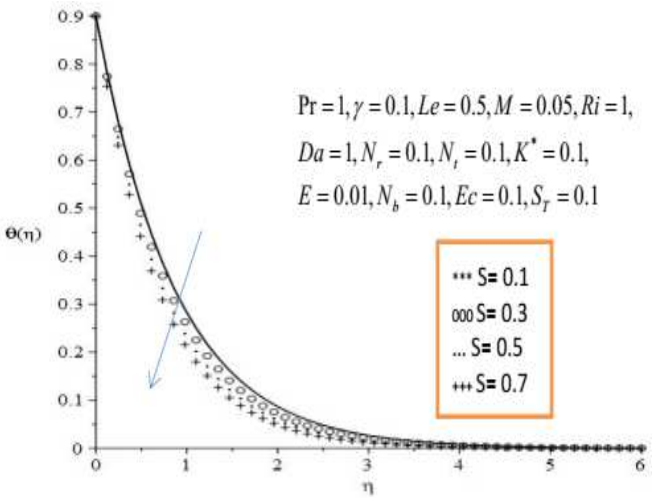

Figure 6: The effect of the suction parameter on the temperature profile.

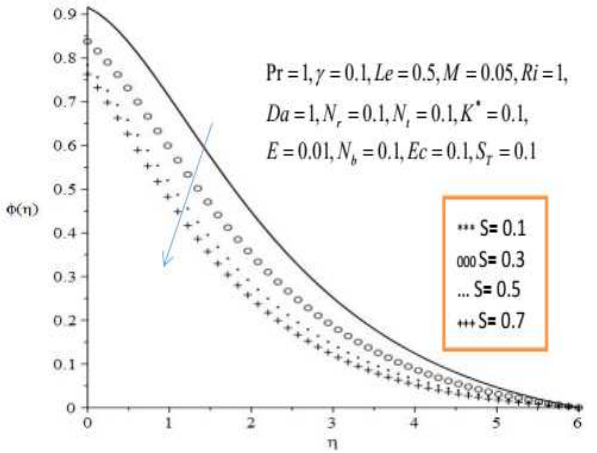

Figure 7: The effect of the suction parameter on the concentration profile.

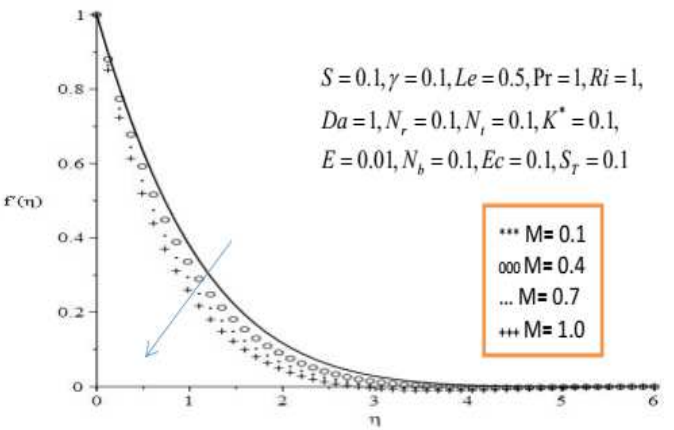

Figure 8: The effect of the magnetic field parameter on the velocity profile.

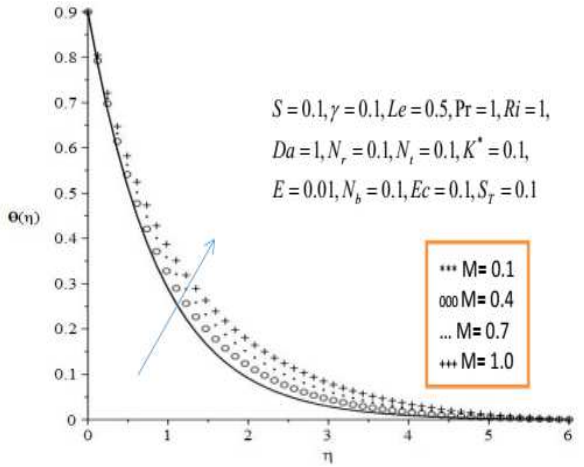

Figure 9: The effect of the magnetic field parameter on the temperature profile.

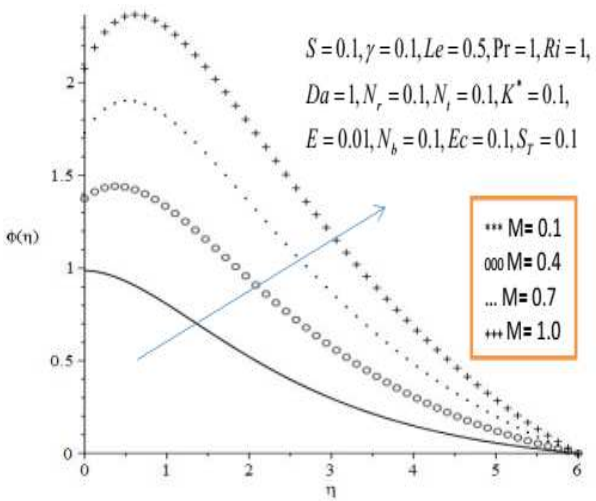

Figure 10: The effect of the magnetic field parameter on the concentration.

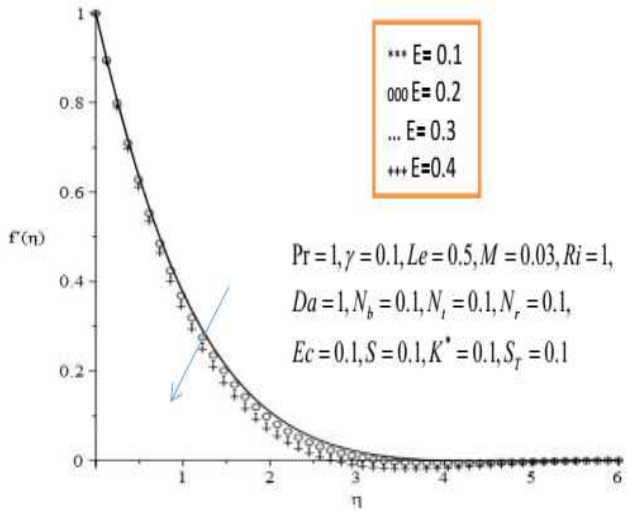

Figure 11: The effect of the electric field parameter on the velocity profile.

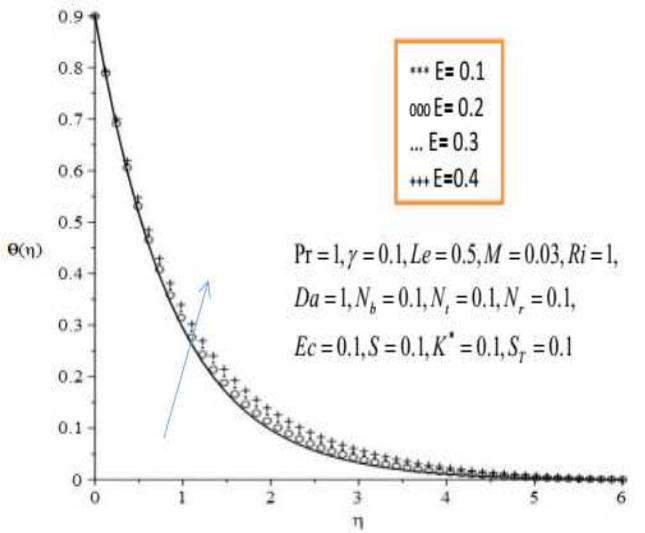

Figure 12: The effect of the electric field parameter on the temperature profile.

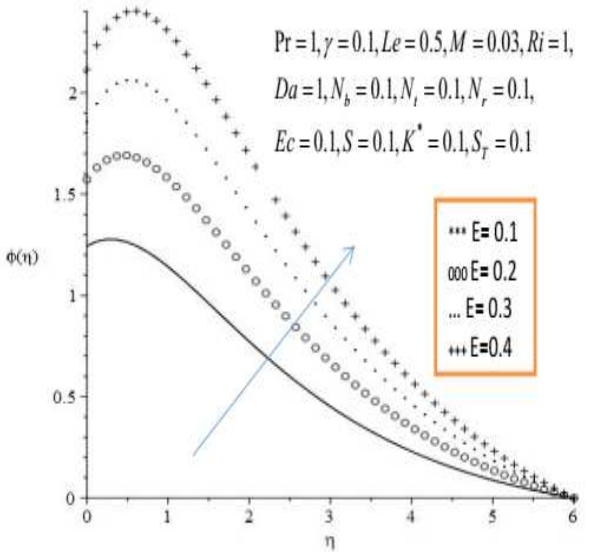

Figure 13: The effect of the electric field parameter on the concentration profile.

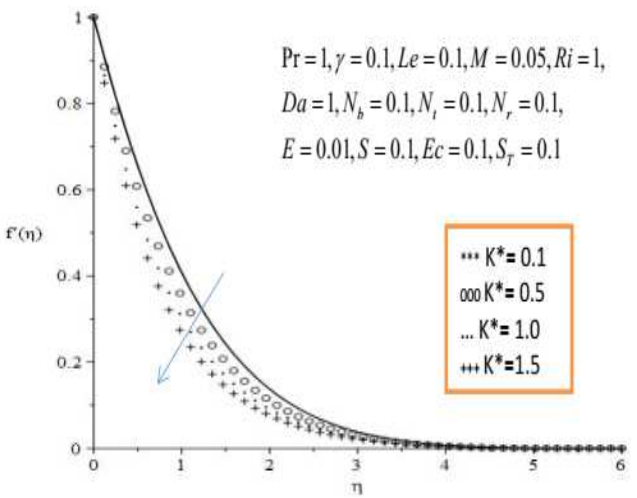

Figure 14: The effect of the permeability parameter on the velocity profile.

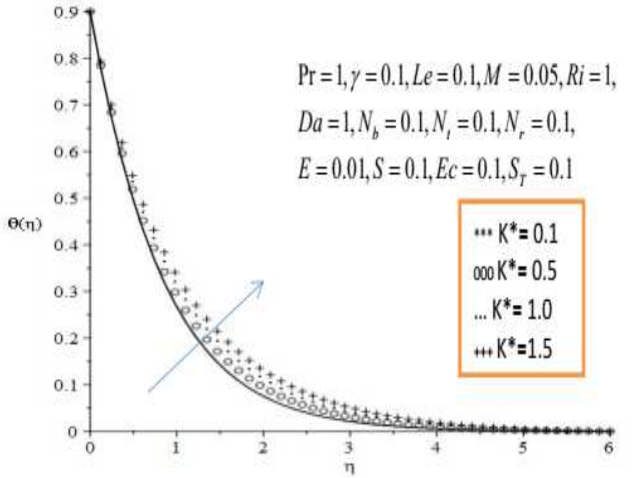

Figure 15: The effect of the permeability parameter on the temperature profile.

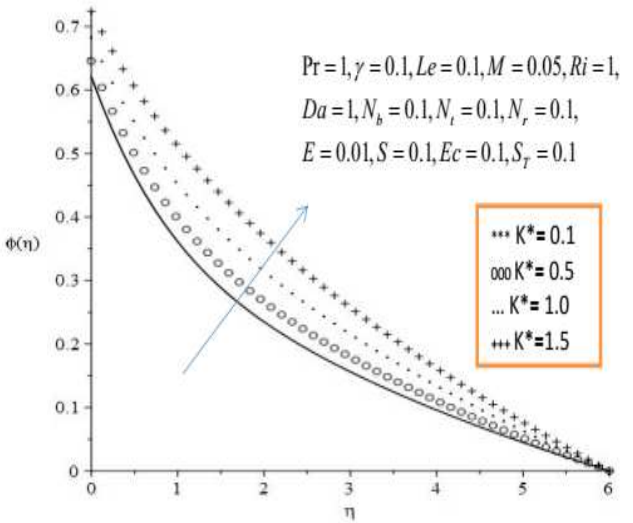

Figure 16: The effect of the permeability parameter on the concentration profile.

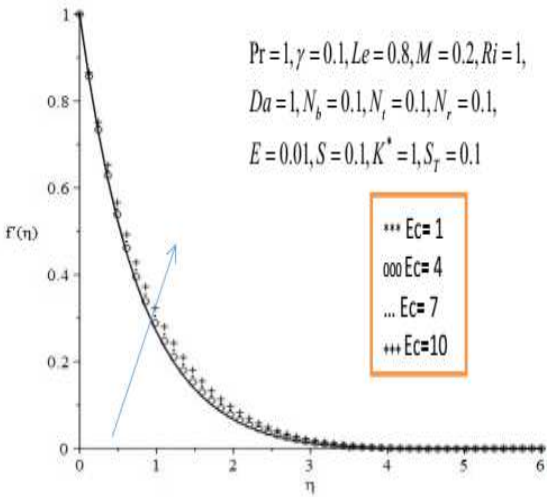

Figure 17: The effect of the Eckert number on the velocity profile.

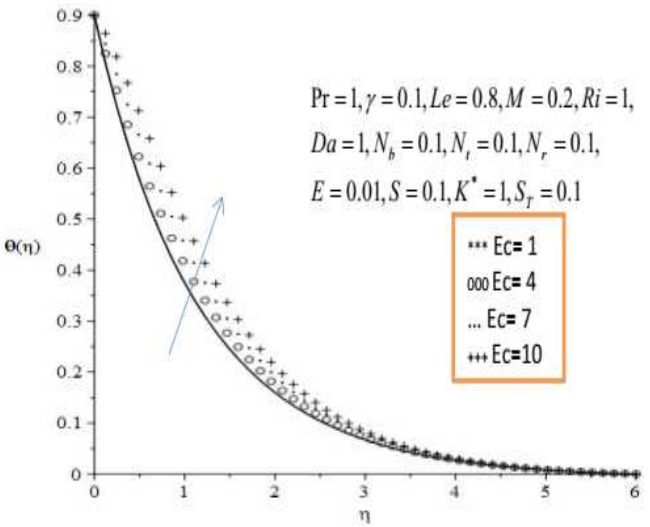

Figure 18: The effect of the Eckert number on the temperature profile.

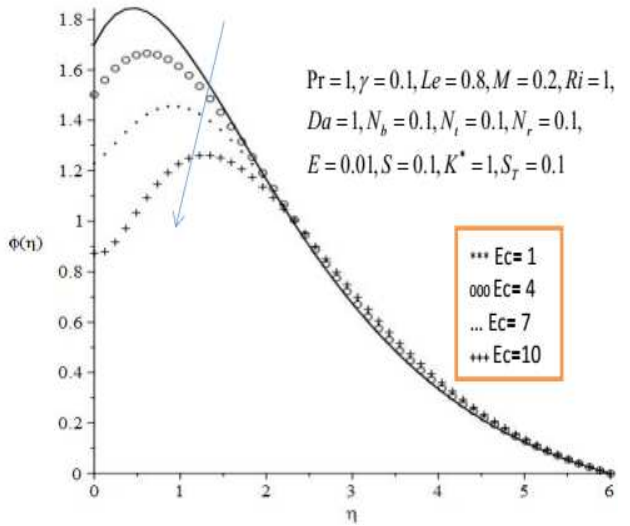

Figure 19: The effect of the Eckert number on the concentration profile.

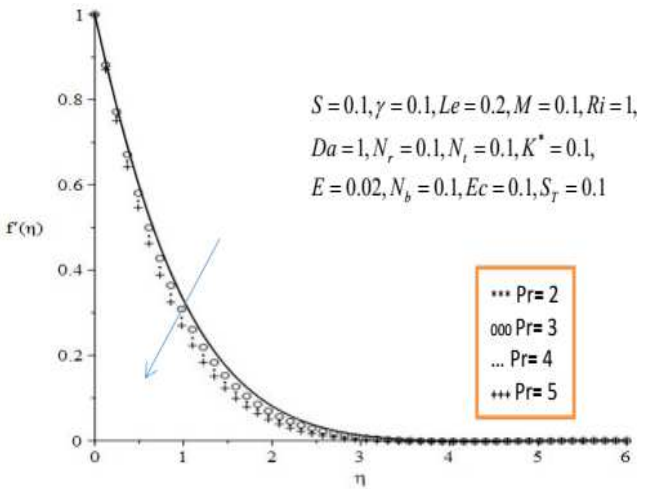

Figure 20: The effect of the Prandtl number on the velocity profile.

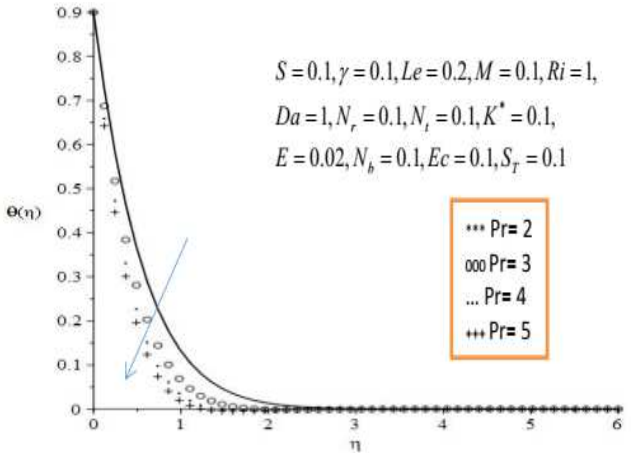

Figure 21: The effect of the Prandtl number on the temperature profile.

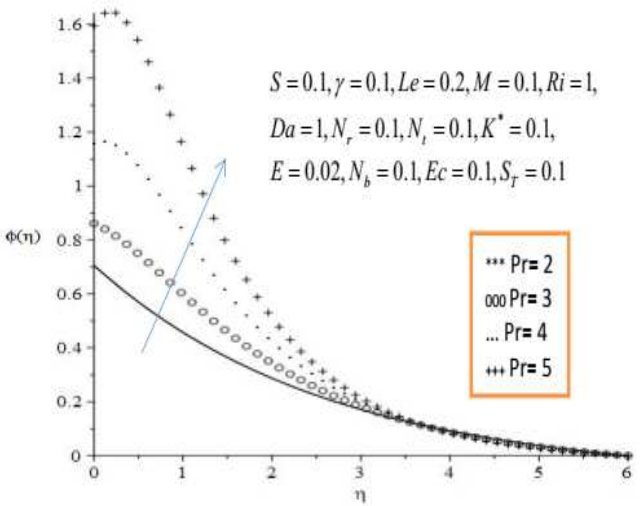

Figure 22: The effect of the Prandtl number on the concentration profile.

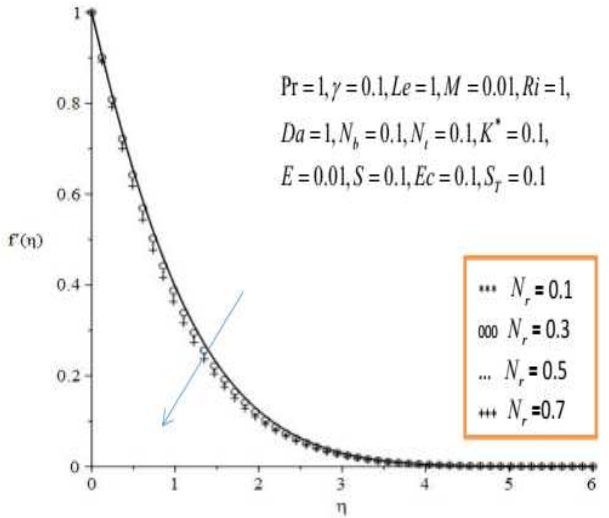

Figure 23: The effect of the Buoyancy ratio parameter on the velocity profile.

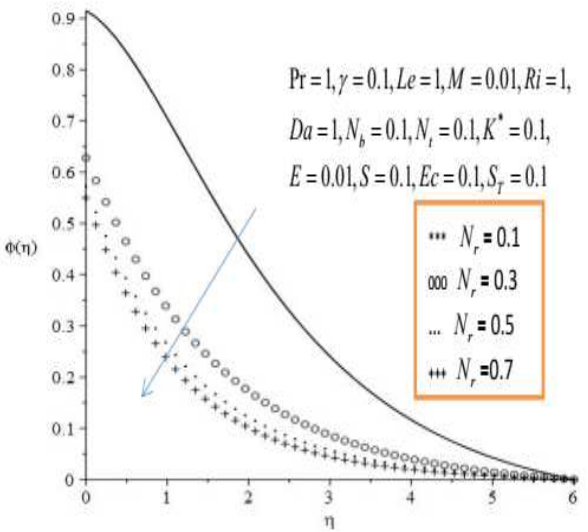

Figure 24: The effect of the Buoyancy ratio parameter on the concentration profile.

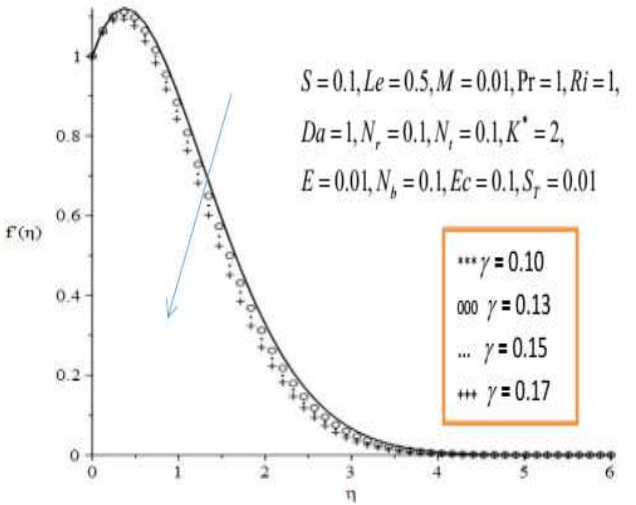

Figure 25: The effect of the Deborah number on the velocity profile.

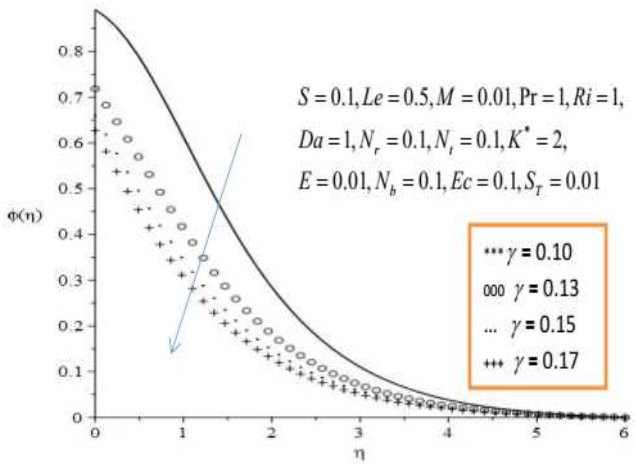

Figure 26: The effect of the Deborah number on the concentration profile.

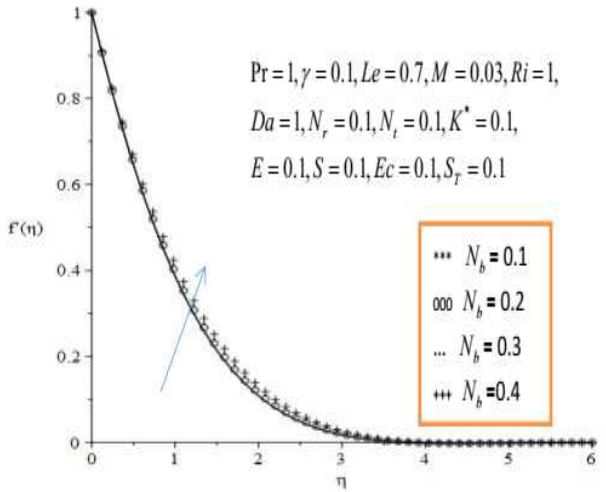

Figure 27: The effect of the Brownian motion parameter on the velocity profile.

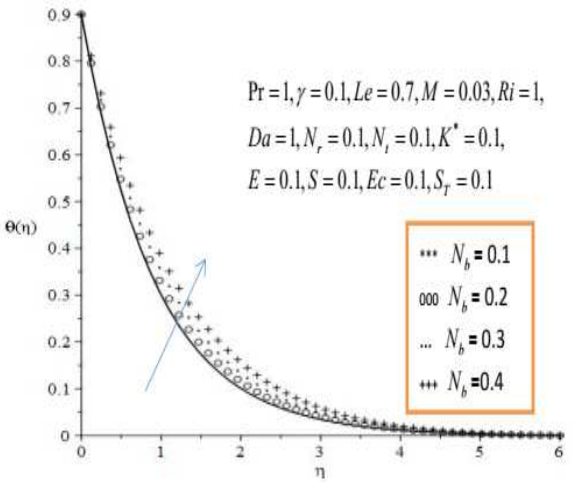

Figure 28: The effect of the Brownian motion parameter on the temperature profile.

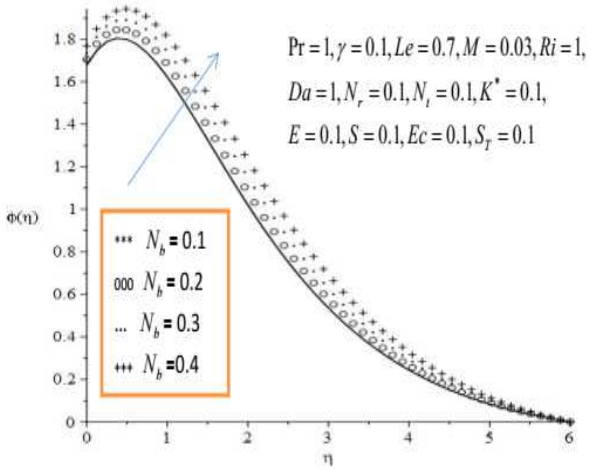

Figure 29: The effect of the Brownian motion parameter on the concentration profile.

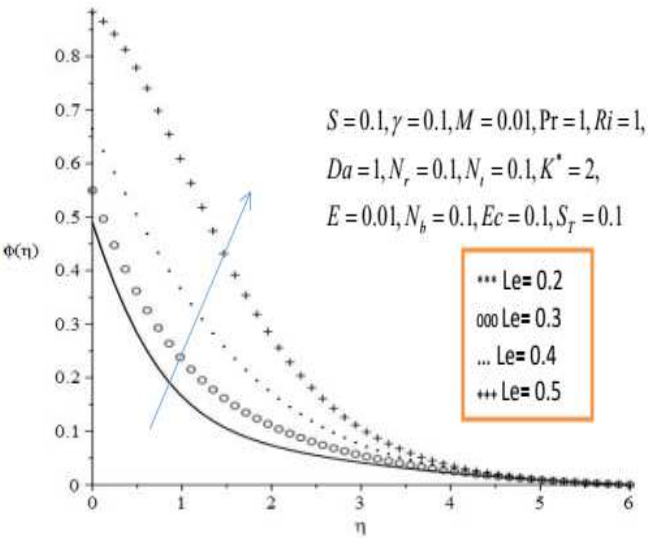

Figure 30: The effect of the Lewis number on the concentration profile.

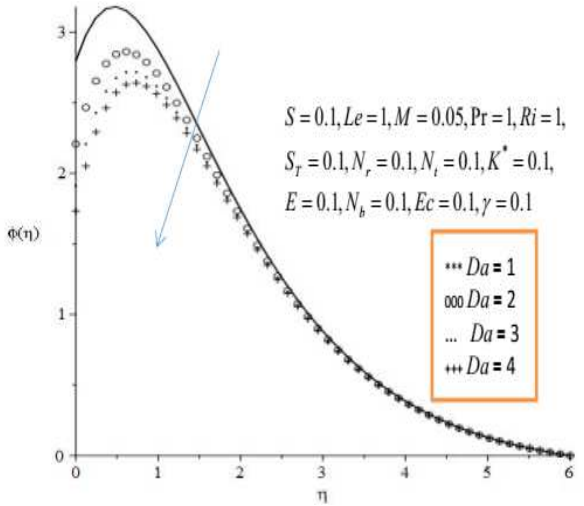

Figure 31: The effect of the Damkohler number on the concentration profile.

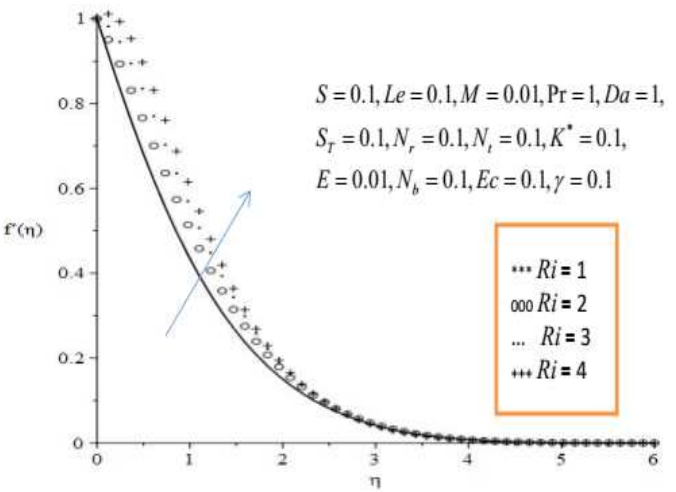

Figure 32: The effect of the Richardson number on the velocity profile.

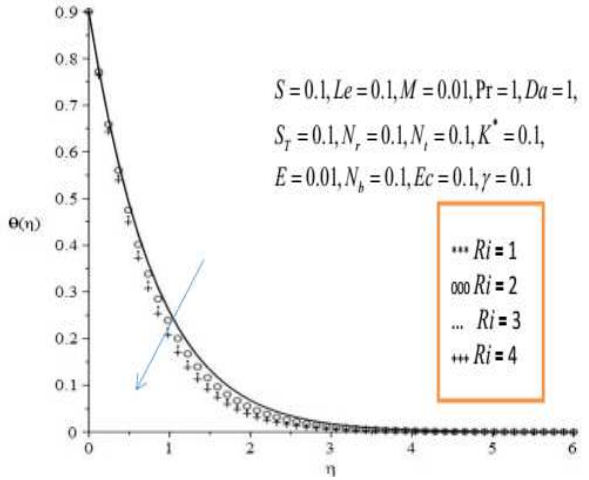

Figure 33: The effect of the Richardson number on the temperature profile.

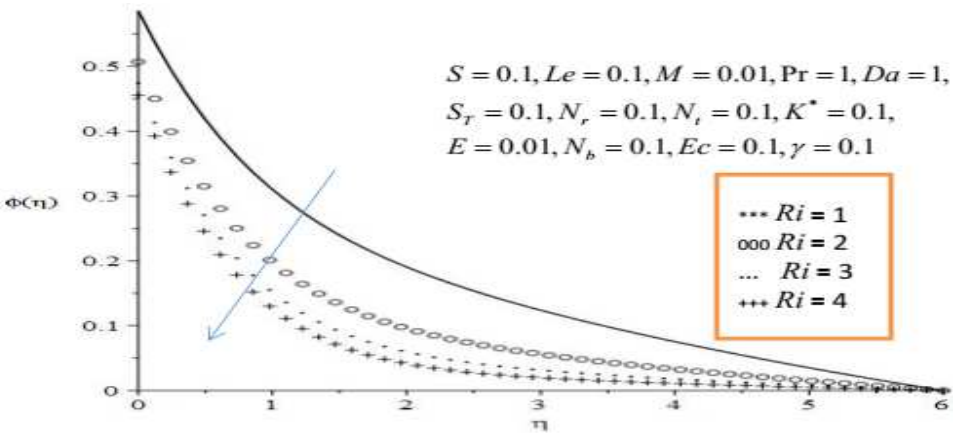

Figure 34: The effect of the Richardson number on the concentration profile.

Conclusions

The effect of thermal stratification on magnetized flow of electrically induced Maxwell nanofluid over reactive stretching plate has been investigated. The partial differential equations modeling the flow were converted into coupled nonlinear differential equation with the aid of similarity transformation. The resulting model was solved using the fourth order Runge Kutta algorithm along with the Shooting technique. The following conclusions can be made:

- Thermal stratification parameter decreased the momentum, thermal and solutal boundary layer thicknesses.
- Magnetic and electric field parameters increased both the thermal and momentum boundary layer thickness while they deteriorated the momentum boundary layer thickness.
- Deborah number depleted both the momentum and solutal boundary layer thicknesses.

Damkohler number enhanced both the Nusselt and Sherwood numbers but it depleted the Skin friction coefficient.

Nomenclature

(x, y) = Cartesian coordinates	Pr = Prandtl number
(u, v) = Velocity components along x and y axes	q_m = Wall mass flux
	C_f = skin-friction coefficient
T_∞ = Free-stream temperature of nanofluid	Re = Reynolds number
T_w = Temperature of the sheet	Nu = Nusselt number
T = Temperature of nanofluid	Sh = Sherwood number
k_s = Thermal conductivity of nanoparticles	q_w = Wall heat flux
k' = Permeability of the porous media	Ec = Eckert number
K^* = Permeability parameter	U_∞ = Free stream velocity of nanofluid
S = Suction parameter	
D_B = Brownian diffusion coefficient	M = Magnetic field parameter
N_b = Brownian motion parameter	E = Electric field parameter
N_r = Buoyancy ratio parameter	Re = Local Reynolds number
N_T = Thermophoresis parameter	Ri = Richardson number
Da = Damkohler number	Gr = Grashof number
C = Concentration of nanofluid	Le = Lewis number
C_∞ = Free stream concentration of nanofluid	S_T = Thermal stratification parameter
h_m = Mass transfer coefficient	D_T = Thermophoresis diffusion coefficient

Symbols

η = Dimensionless Variable	ϕ = Dimensionless Concentration
τ_w = Wall shear stress	λ_1 = Time relaxation parameter
υ_f = Kinematic viscosity of nanofluid	$(\rho C)_p$ = Heat capacity of nanofluid
ρ_f = Density of nanofluid	β = Volume expansion coefficient
ρ_p = Density of nanoparticles	γ = Deborah number
$(\rho C)_f$ = Heat capacity of nanofluid	μ_f = Dynamic viscosity of nanofluid
ψ = Stream function	α_f = Thermal diffusivity of nanofluid
θ = Dimensionless Temperature	σ = Electrical conductivity

References

[1] M. Ramzan, M. Bilal, J.D. Chung and U. Farooq, Mixed convective flow of Maxwell nanofluid past a porous vertical stretched surface – An optimal solution, *Results in Physics* 6 (2016), 1072-1079. https://doi.org/10.1016/j.rinp.2016.11.036

[2] W. Ibrahim, Magnetohydrodynamic stagnation point flow and heat transfer of upper-convected Maxwell fluid past a stretching sheet in the presence of nanoparticles with convective heating, *Frontiers in Heat and Mass Transfer (FHMT)* 7(4) (2016), 1-10. https://doi.org/10.5098/hmt.7.4

[3] E.M.A.R. Elbashbeshy, K.M. Abdelgaber and H.G. Asker, Heat and mass transfer of a Maxwell nanofluid over a stretching surface with variable thickness embedded in porous medium, *International Journal of Mathematics and Computational Science* 4(3) (2018), 86-98.

[4] A. Mushtaq, M. Mustafa, T. Hayat and A. Alsaedi, Buoyancy effects in stagnation-point flow of Maxwell fluid utilizing non-Fourier heat flux approach, *PLoS ONE* 13(5) (2018), 1-19. https://doi.org/10.1371/journal.pone.0192685

[5] C.S. Sravanthi and R.S.R. Gorla, Effects of heat source/sink and chemical reaction on MHD Maxwell nanofluid flow over a convectively heated exponentially stretching sheet using homotopy analysis method, *Int. J. Applied Mechanics and Engineering* 23(1) (2018), 137-159. https://doi.org/10.1515/ijame-2018-0009

[6] V.J. Sushma, B.T. Raju, L.N. Achala and S.B. Sathyanarayana, Study of Maxwell nanofluid flow over a stretching sheet with non-uniform heat source/sink with external magnetic field, *Journal of Advanced Research in Fluid Mechanics and Thermal Sciences* 55(2) (2019), 218-232.

[7] S.E. Ahmed, R.A. Mohamed, A.E.M. Aly and M.S. Soliman, Magnetohydrodynamic

Maxwell nanofluids flow over a stretching surface through a porous medium: effects of non-linear thermal radiation, convective boundary conditions and heat generation/ absorption, *International Journal of Aerospace and Mechanical Engineering* 13(6) (2019), 436-443.

[8] U. Farooq, D. Lu, S. Munir, M. Ramzan, M. Suleman and S. Hussain, MHD flow of Maxwell fluid with nanomaterials due to an exponentially stretching surface, *Scientific Report* (2019), 1-11. https://doi.org/10.1038/s41598-019-43549-0

[9] A. Aziz and M. Shams, Entropy generation in MHD Maxwell nanofluid flow with variable thermal conductivity, thermal radiation, slip conditions and heat source, *AIP Advances* 10(015038) (2020), 1-12. https://doi.org/10.1063/1.5129569

[10] W. Ibrahim and M. Negera, MHD slip flow of upper-convected Maxwell nanofluid over a stretching sheet with chemical reaction, *Journal of the Egyptian Mathematical Society* 28(7) (2020), 1-28. https://doi.org/10.1186/s42787-019-0057-2

[11] K. Singh and M. Kumar, The effect of chemical reaction and double stratification on MHD free convection in a micropolar fluid with heat generation and ohmic heating, *Jordan Journal of Mechanical and Industrial Engineering* 9(4) (2015), 279-288.

[12] F.M. Abbasi, S.A. Shehzad, T. Hayat and B. Ahmad, Doubly stratified mixed convection flow of Maxwell nanofluid with heat generation/absorption, *Journal of Magnetism and Magnetic Materials* 404 (2016), 159-165. https://doi.org/10.1016/j.jmmm.2015.11.090

[13] N.V. Ganesh, A.K.A. Hakeem and B. Ganga, Darcy-Forchheimer flow of hydromagnetic nanofluid over a stretching/shrinking sheet in a thermally stratified porous medium with second order slip, viscous and Ohmic dissipations effects, *Ain Shams Eng. J.* 9 (2016), 939-951. https://doi.org/10.1016/j.asej.2016.04.019

[14] M. Ramzan, M. Bilal and J.D. Chung, Radiative flow of Powell-Eyring magneto-nanofluid over a stretching cylinder with chemical reaction and double stratification near a stagnation point, *PLoS ONE* 12(1) (2017), 1-19. https://doi.org/10.1371/journal.pone.0170790

[15] Y.S. Daniel, Z.A. Aziz, Z. Ismail and F. Salah, Thermal stratification effects on MHD radiative flow of nanofluid over nonlinear stretching sheet with variable thickness, *Journal of Computational Design and Engineering* 5 (2018), 232-242. https://doi.org/10.1016/j.jcde.2017.09.001

[16] K. Sreelakshmi, G. Sarojamma and O.D. Makinde, Dual stratification on the Darcy-Forchheimer flow of a Maxwell nanofluid over a stretching surface, *Defect and Diffusion Forum* 387 (2018), 207-217. https://doi.org/10.4028/www.scientific.net/DDF.387.207

[17] M. Farooq, S. Ahmad, M. Javed and A. Anjum, Magnetohydrodynamic flow of squeezed Maxwell nano-fluid with double stratification and convective conditions, *Advances in Mechanical Engineering* 10(9) (2018), 1-13. https://doi.org/10.1177/1687814018801140

[18] M. Ramzan, N. Shaheen, S. Kadry, Y. Ratha and Y. Nam, Thermally stratified Darcy Forchheimer flow on a moving thin needle with homogeneous heterogeneous reactions and non-uniform heat source/sink, *Appl. Sci.* 10(432) (2020), 1-14. https://doi.org/10.3390/app10020432

[19] N.S. Khashi, E.H. Hafidzuddin, N. Md. Arifin and N. Wahi, Stagnation point flow of hybrid nanofluid over a permeable vertical stretching/shrinking cylinder with thermal stratification effect, *CFD Letters* 12(2) (2020), 80-94.

[20] R.S.R. Gorla and I. Sidawi, Free convection on a vertical stretching surface with suction and blowing, *Applied Scientific Research* 52(3) (1994), 247-257. https://doi.org/10.1007/BF00853952